Applied Catalysis B: Environmental 179 (2015) 313–320

Contents lists available at ScienceDirect

Applied Catalysis B: Environmental

journal homepage: www.elsevier.com/locate/apcatb

# Improved catalytic methane combustion of Pd/$CeO_2$ catalysts via porous glass integration

Martina Hoffmann[a], Stefanie Kreft[a], Gabriele Georgi[a], Gerhard Fulda[b], Marga-Martina Pohl[a], Dominik Seeburg[a], Claudia Berger-Karin[a,1], Evgenii V. Kondratenko[a], Sebastian Wohlrab[a,*]

[a] Leibniz Institute for Catalysis at the University of Rostock, Albert-Einstein-Str. 29a, D-18059 Rostock, Germany
[b] Electron Microscopy Center, Strempelstr. 14, University Medicine, D-18057 Rostock, Germany

ARTICLE INFO

*Article history:*
Received 2 January 2015
Received in revised form 7 May 2015
Accepted 12 May 2015
Available online 15 May 2015

*Keywords:*
Methane oxidation
Exhaust gas
Low temperature
Long term stability
Catalyst reducibility

ABSTRACT

Methane combustion catalysts composed of Pd and $CeO_2$ were synthesized through impregnation of porous glasses with cerium nitrate melt and palladium nitrate solution followed by subsequent calcination. They were tested in the temperature range from 150 to 550 °C using a feed with 1.0 vol% methane in air at a GHSV (gas hourly space velocity) of ~30,000 $h^{-1}$. The catalyst prepared with a glass possessing a pore diameter of 151 nm and a Pd loading of 0.63 wt% completely converted methane at 350 °C compared to 415 °C required for a classically prepared Pd/$CeO_2$ reference. The novel catalyst also showed superior on stream stability as proven in 50 h tests. The influence of preparation method, pore size of the glass supports and Pd loading on the activity for $CH_4$ total oxidation was further investigated and correlated with the results of $H_2$-TPR and CO chemisorption. It is suggested that the catalyst activity for methane combustion is determined by both (i) Pd particle size and (ii) surface reducibility of $CeO_2$.



## 1. Introduction

In the past decades, anthropogenic emissions of greenhouse gases contributing to global warming have strongly increased. One of such gases is methane possessing a 25 times higher global warming potential than carbon dioxide [1]. It is mostly released from industrial processes, agriculture, and waste management but the abatement of such emissions is yet not industrially realized since economically feasible approaches are still missing. Novel methane-based technologies will even aggravate this problem. For example, beside the production of thermal energy, methane as fuel in natural-gas vehicles presents a highly desirable alternative to currently used gasoline or diesel [2]. However, the exhaust gas stream from natural gas engines also contains unburned methane. Consequently, an increase in methane emissions in the future can be expected. One approach to control such emissions is the catalytic oxidation of methane to carbon dioxide. For this purpose, it is highly important that catalytic materials completely oxidize methane at temperatures as low as possible and show high on stream stability.

Potential candidates for this purpose are supported catalysts possessing palladium or platinum as active components [3]. Their activity can be tuned by support materials. Especially, catalysts based on redox-active metal oxide supports show high activity and on stream stability [4–6]. In an earlier study, Farrauto et al. [7] investigated the influence of metal oxide supports on the reduction of PdO and the reoxidation of Pd to PdO. These both processes play an important role in the course of methane combustion [7]. $CeO_2$ used as support for $PdO_x$ was found to show the smallest hysteresis effect during this redox cycle. Over the years, the most active catalysts are indeed based on differently prepared $CeO_2$ supports. For example, Xiao et al. [8] reported on 100% methane conversion at 300 °C and a GHSV (gas hourly space velocity) of 50,000 $h^{-1}$ over Pd (2.0 wt%)/$CeO_2$ prepared by a deposition–precipitation method. However, this catalyst lost around 7% of its initial conversion during first 16 h on stream. Another very effective catalytic system developed by Yasuda et al. [9] is Pd (10 wt%)/$CeO_2$–$ZrO_2$–$Bi_2O_3$/γ-$Al_2O_3$ reaching complete methane conversion at 320 °C and a GHSV of 20,000 $h^{-1}$. Unfortunately, the high Pd loading is rather unattractive from an industrial viewpoint. In both cases, a lean methane–air mixture (1 vol% $CH_4$ in air) was used simulating emissions resulting from natural gas combustion engines. Very recently Cargnello

* Corresponding author. Tel.: +49 381 1281 328; fax: +49 381 1281 51 328.
*E-mail address:* sebastian.wohlrab@catalysis.de (S. Wohlrab).
[1] Present Address: ILS-Integrated Lab Solutions GmbH, Max-Planck-Straße 3, 12489 Berlin, Germany.

http://dx.doi.org/10.1016/j.apcatb.2015.05.028
0926-3373/

**Table 1**
Characteristics of the glass supports and amount of Ce precursor used for Pd*X*/$CeO_2$/PG*Y* preparation.

| Glass No. | PG27 | PG63 | PG151 |
|---|---|---|---|
| Average pore size [nm][a] | 27 | 63 | 151 |
| Granule diameter [μm][a] | 74–160 | 130–200 | 100–200 |
| Avg. pore volume [$cm^3\ g^{-1}$][a] | 1.14 | 1.33 | 1.53 |
| Specific surface area [$m^2\ g^{-1}$] | 199.8 | 62.0 | 21.8 |
| m($Ce(NO_3)_3 \cdot 6H_2O$) [$g/g_{glass}$] | 3.26 | 3.80 | 4.36 |

[a] Given by the manufacturer.

et al. [10] introduced a novel catalyst with core–shell structures of 2.0 wt% palladium in porous ceria on hydrophobic alumina. This catalyst showed high thermal stability and complete methane conversion at 400 °C using a feed consisting of 0.5 vol% $CH_4$ and 2 vol% $O_2$ in He.

Apart from metal oxides, porous structures such as SBA-15 [11,12], HMS [12] and zeolites [13] have received notable interest as supports for Pd. However, in such porous materials, Pd particle size being an important activity-governing factor is restricted to the small pore sizes of the supports thus limiting additional loading of a redox active metal oxide. Alternatively, supports with pore sizes starting from the upper mesopore region can provide suitable frameworks for dispersing catalytically active $CeO_2$ and $Pd/PdO_x$ onto their inner surfaces. Porous glasses belong to such materials. They are usually manufactured from phase-separated borosilicate glasses by extraction and contain more than 96 wt% silica [14]. Until now porous glasses are not often applied as supports even though their structural properties like surface area, pore size and pore volume can be easily tuned [15]. Only some implementations as catalysts or supports are known, *e.g.* as catalytic membranes in cyclohexane dehydrogenation [16], coupling reactions [17], and conversions of alcohols, as the oxidation of ethylene glycol to glycolic acid [18,19].

The aim of the present study was to explore the potential of porous glasses as supports for $Pd/PdO_x$ and $CeO_2$ species to prepare catalysts for complete methane combustion. Particularly, we investigated influences of different impregnation methods, pore sizes of glasses and palladium loading on the average size of Pd species and the redox properties of $CeO_2$. These two characteristics were related to catalyst activity.

## 2. Experimental

### 2.1. Synthesis of $Pd/CeO_2$ catalysts in porous glasses

Glasses with an average pore diameter of 27, 63, or 151 nm were purchased from VitraBio GmbH (Germany). Their selected structural characteristics are summarized in Table 1. The $SiO_2$ content in all glasses was higher than 96 wt%. Further components were $B_2O_3$ (2.5–3.5 wt%), $Na_2O$ (0.2–0.5 wt%) and traces of $Al_2O_3$. Two different approaches were used for catalyst preparation, *i.e.*, glasses were simultaneously (SI) or consecutively (CI) impregnated with sources of Pd and Ce. In the SI method, granules of porous glasses were immersed into a mixture of molten $Ce(NO_3)_3 \cdot 6H_2O$ (Sigma–Aldrich, 99%) and $Pd(NO_3)_2 \cdot 2H_2O$ (Merck) at 235 °C. The required amount of $Ce(NO_3)_3 \cdot 6H_2O$ was calculated to completely fill the glass pores considering a melt density of 2.38 g $cm^{-3}$ (measured using a pycnometer), while the amount of the Pd salt was set to have 1 wt% Pd with respect to $CeO_2$.

According to the CI method, glass granules were initially impregnated with pure molten $Ce(NO_3)_3 \cdot 6H_2O$ and calcined at 450 °C at a heating rate of 5 °C $min^{-1}$ for 2 h yielding a pore filling degree of 15 vol% considering the density of $CeO_2$ of 7.3 g $cm^{-3}$. Hereafter, the obtained $CeO_2$-containing glasses were impregnated with a $Pd(NO_3)_2 \cdot 2H_2O$ solution via the incipient wetness impregnation method to yield catalysts with 1, 5 or 10 wt% Pd with respect to $CeO_2$. $Pd(NO_3)_2 \cdot 2H_2O$ was dissolved in water with a volume necessary for a complete filling of the remaining pore volume of the obtained $CeO_2$-impregnated glasses. Finally, the catalyst precursors were dried in air at 60 °C for 60 min and calcined at 500 °C (heating rate of 5 °C $min^{-1}$) for 1 h. Catalysts are abbreviated according to the following nomenclature: Pd*X*/$CeO_2$/PG*Y* with *X*: Amount of Pd related to $CeO_2$ in wt% and *Y*: average pore diameter of the porous glass support. To distinguish the catalyst prepared through the SI method from those synthesized through the CI method, we added "si" before the catalyst abbreviation, *i.e.* si-Pd1/$CeO_2$/PG151.

For comparison, a Pd1/$CeO_2$ reference catalyst (1 wt% Pd related to $CeO_2$) was synthesized without the glass support according to the following protocol. $Ce(NO_3)_3 \cdot 6H_2O$ was calcined in air at 450 °C (heating rate of 5 °C $min^{-1}$) for 1 h to yield $CeO_2$. The latter was impregnated with a $Pd(NO_3)_2 \cdot 2H_2O$ solution *via* the incipient wetness method to yield 1 wt% Pd in the final catalyst after drying in air at 60 °C for 60 min and calcination at 500 °C (heating rate of 5 °C $min^{-1}$) for 1 h.

Pd1/10$CeO_2$/PG151 was tenfold impregnated with $Ce(NO_3)_3 \cdot 6H_2O$ according to the available free space in the glass. After each impregnation step the material was calcined in air at 450 °C (heating rate 5 °C $min^{-1}$) for 2 h and finally calcined at 900 °C. After incipient wetness impregnation with aqueous $Pd(NO_3)_2 \cdot 2H_2O$ the catalysts were dried in air at 60 °C for 60 min and calcined at 500 °C (heating rate of 5 °C $min^{-1}$) for 1 h.

Pd1/PG151 was prepared by impregnation with a $Pd(NO_3)_2 \cdot 2H_2O$ solution (1 wt% Pd related to $SiO_2$) and subsequent drying and calcination as described for Pd*X*/$CeO_2$/PG*Y* catalysts.

### 2.2. Catalytic testing for $CH_4$ combustion

Catalytic tests were performed in a vertical fixed-bed plug-flow quartz tubular reactor (inner diameter of 6 mm) at ambient pressure. The catalyst (0.2 g; granule diameter: see Table 1) was placed in the isothermal reactor zone and fixed by quartz wool located downstream below the catalyst bed. The catalytic activity was measured starting from 150 °C with a step-wise increase in temperature of 25 or 50 K until full conversion of methane was achieved. At each temperature methane conversion was recorded threefold within 30 min using an on-line gas chromatograph equipped with a methanizer for flame ionization detection and a thermal conductivity detector. The feed components as well as the reaction products were detected, except water.

In separate experiments, Pd10/$CeO_2$/PG151, Pd1/$CeO_2$/PG151 and Pd1/$CeO_2$ were tested under isothermal conditions at $T_{20}$, $T_{100}$ (the specific temperatures necessary for 20% or 100% methane conversion, respectively) as well as at 525 °C over 50 h on stream. In all tests, the reactant gas stream consisted of methane, oxygen and nitrogen in the ratio of 1:18:81 representing a feed with 1.0 vol% $CH_4$ in air. The total flow rate was 75 $cm^3\ min^{-1}$ to yield a GHSV of ~30,000 $h^{-1}$.

### 2.3. Analytical methods

X-ray diffraction (XRD) measurements were performed on a STADI P transmission diffractometer from STOE (Darmstadt, Germany). The samples were ground and afterwards analyzed applying a curved germanium monochromator in the incident beam path, CuKα radiation (λ = 0.15406 nm) and a 6° linear position sensitive detector (PSD). The Scherrer equation [20] was used to calculate the size of $CeO_2$ crystallites from the (1 1 1) reflex at 2θ of *ca.* 28.5.

**Table 2**
Characteristics of the prepared Pd*X*/$CeO_2$/PG*Y* catalysts.

| Catalyst | Pd content [wt%][a] | Pd surface area, $S_{Pd}$ [$m^2\,g^{-1}$][b] | Pd particle size, *d* [nm][b] | Dispersion [%] | $CeO_2$ content [wt%] | $CeO_2$ crystallite size [nm][c] | $S_{BET}$ [$m^2\,g^{-1}$] | $TOF_{CH4}$ [$s^{-1}$] at 250 °C |
|---|---|---|---|---|---|---|---|---|
| Pd1/$CeO_2$/PG151 (after 50 h on stream) | 0.63(0.62) | 1.17(1.20) | 2.6(2.6) | 43 | 62.9 | 22 | 81.6 | $1.29 \times 10^{-2}$ |
| Pd1/$CeO_2$ (after 50 h on stream) | 0.99(1.00) | 2.86(3.03) | 1.6(1.6) | 64 | 99.0 | 21 | 116.4 | $2.04 \times 10^{-3}$ |
| Pd1/$CeO_2$/PG63 | 0.60 | 1.86 | 1.6 | 64 | 59.8 | 21 | 81.3 | $9.2 \times 10^{-4}$ |
| Pd1/$CeO_2$/PG27 | 0.56 | 2.04 | 1.4 | 70 | 56.0 | 21 | 127.4 | $3.30 \times 10^{-3}$ |
| Pd5/$CeO_2$/PG151 | 3.07 | 5.58 | 2.8 | 40 | 61.4 | 17 | 80.0 | $3.19 \times 10^{-3}$ |
| Pd10/$CeO_2$/PG151 | 5.96 | 5.47 | 5.6 | 20 | 59.6 | 17 | 75.5 | $1.00 \times 10^{-2}$ |

[a] Obtained from ICP.
[b] Calculated from dynamical CO chemisorption carried out at room temperature assuming that one CO is adsorbed on one Pd.
[c] Estimated from XRD measurements using the Scherrer equation for the (1 1 1) reflex.

The BET specific surface area ($S_{BET}$) of the catalyst samples was measured by nitrogen adsorption using a NOVA 4200e instrument from Quantachrome (Odelzhausen, Germany).

TEM (transmission electron microscopy) measurements at 200 kV were performed on a JEM-ARM200F (JEOL) with aberration-correction by a CESCOR (CEOS) for the scanning transmission (STEM) applications.

The pore structure of the porous glass granules was imaged by SEM (scanning electron microscopy) using a JEOL 7401F instrument. Catalysts were further investigated by means of EDX (energy dispersive X-ray) analysis using a Zeiss DSM960A und a Zeiss Merlin VP compact. To check if carbon deposits were formed over Pd10/$CeO_2$/PG151, Pd1/$CeO_2$/PG151 and Pd1/$CeO_2$ during the 50 h test at $T_{100}$, these used catalysts were analyzed using a Micro-analysator TruSpec CHNS (Leco Corporation, USA).

A Varian 715-ES ICP-OES (Inductively Coupled Plasma-Optical Emission Spectrometer) was used for the determination of the elemental composition of the catalysts after complete dissolution in a solution containing 8 mL of aqua regia and 2 mL hydrofluoric acid.

Dynamical CO chemisorption was carried out with an AutoChem 2920 device (Micromeritics, Aachen, Germany). Before the chemisorption tests, the samples were initially pretreated in flow of 5 vol% $O_2$ in He at 300 °C followed by reduction in hydrogen (5 vol% $H_2$ in Ar) at the same temperature. Hereafter the reduced samples were cooled in an Ar flow to room temperature. Afterwards pulses (500 μl) of 20 vol% CO/He were given into a He flow. Saturation of the palladium surface was observed by constant CO peaks by means of a thermal conductivity detector (TCD). Palladium dispersion was calculated assuming that one CO molecule is adsorbed on one Pd surface atom and Pd surface density of $1.27 \times 10^{19}$ atoms $m^{-2}$ was assumed for the calculation of Pd surface area, $S_{Pd}$. The Pd particle sizes were calculated according the equation $d = 6\,V_{Pd}/S_{Pd}$ assuming an atomic volume $V_{Pd}$ of $7.9 \times 10^{-29}$ $m^3$ $atom^{-1}$ [21,22].

Prior to temperature-programmed reduction ($H_2$-TPR) experiments, the tested samples were heated in air to 500 °C and then cooled to room temperature in the same flow. Temperature-programmed reduction ($H_2$-TPR) experiments were carried out as follows. 50 mg of each sample were filled into fixed-bed quartz tubular reactors (inner diameter of 6 mm) and heated in air to 500 °C and then cooled to room temperature in the same flow. Hereafter, the reactors were purged with a flow of Ar for 30 min followed by feeding an $H_2$:Ar = 5:95 flow and then heating to 650 °C with a temperature ramp of 10 °C $min^{-1}$. Final temperature was held for 15 min followed by cooling down to 50 °C in an air flow of 10 ml $min^{-1}$. The total gas flow of the $H_2$-containing mixture amounted to 10 ml $min^{-1}$, fulfilling the criterion of Monti and Baiker [23]. Hydrogen consumption and water formation were monitored by an on-line quadrupole mass spectrometer (OmniStar, Pfeiffer Vacuum, Germany).

## 3. Results and Discussion

### 3.1. Structural properties of catalytic materials

XRD patterns of the Pd*X*/$CeO_2$/PG*Y* catalysts are similar to those of unsupported Pd1/$CeO_2$ and evidence the presence of crystalline $CeO_2$ (see Fig. S1). The estimated average size of $CeO_2$ particles was between 17 and 23 nm for all catalysts (Table 2). Neither Pd nor PdO were detected in oxidized samples. The reduced counterparts were not analyzed by XRD.

The specific surface areas of unloaded glasses and catalytic materials are listed in Table 1 and Table 2, respectively. Interestingly, the surface areas of PG151 and PG63 increased from 21.8 to 81.6 $m^2\,g^{-1}$ and from 62.0 to 81.3 $m^2\,g^{-1}$ after impregnation, respectively, while the surface area of PG27 decreased from 199.8

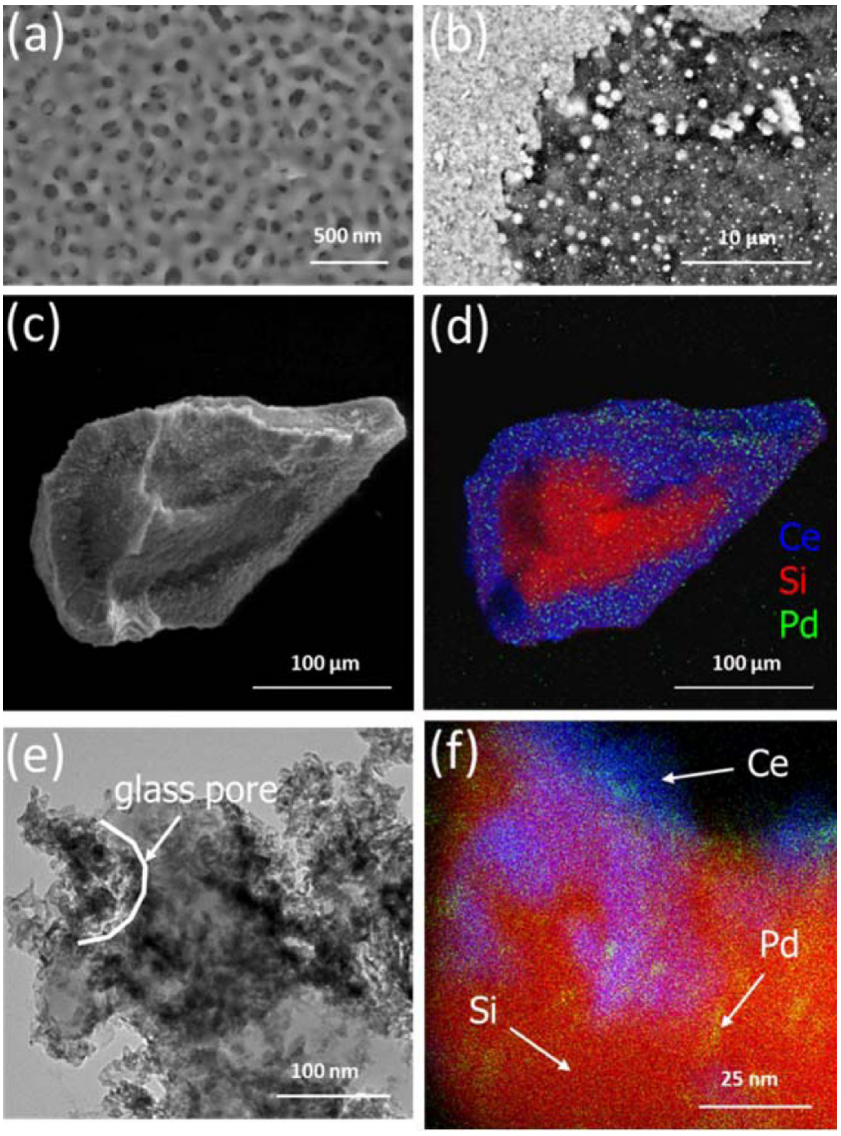


**Fig. 1.** Electron microscopy on Pd1/$CeO_2$/PG151; (a) SEM image; pore structure of pure PG151. (b) Backscattered electron image; interface between near surface $CeO_2$ and the granule core. (c) SEM image; fracture. (d) SEM-EDX mapping. (e) TEM image; $CeO_2$ particles adhering to the glass pore walls. (f) TEM-EDX mapping; (Ce – blue, Si – red, Pd – green). (For interpretation of the references to color in this figure legend, the reader is referred to the web version of this article.)

to 121.7 $m^2\ g^{-1}$. From a general viewpoint, the effect of impregnation on the surface area depends on two competing factors: (i) an increase in surface area due to the generation of small $CeO_2$ particles inside the glass pores and (ii) a decrease in accessible surface area due to the blocking of glass pores as a consequence of $CeO_2$ formation inside the pores. In case of PG151, the average pore diameter of 151 nm is high enough to exclude pore blockage by 22 nm $CeO_2$ particles. Therefore, the surface area of Pd1/$CeO_2$/PG151 increases due to the presence of added $CeO_2$. Compared to this catalyst, the positive effect of $CeO_2$ addition on the surface area of Pd1/$CeO_2$/PG63 is less pronounced since the pore size in PG63 is significantly smaller than in PG151 (Table 1). Consequently, some pores can be blocked by $CeO_2$. This blocking process is responsible for the decrease in the surface area of PG27 after impregnation, as $CeO_2$ particle size and glass pore size are nearly identical.

Fig. 1a shows a SEM image representatively illustrating the framework structure of the non-impregnated PG151 glass. All pores are interconnected and relatively uniform in size. As seen from the SEM and EDX-SEM images of Pd1/$CeO_2$/PG151 in Fig. 1b–d, the impregnation did not result in a homogeneous filling of the glass pores. Despite the fact that a complete pore filling with cerium nitrate melt was initially achieved, the formation of nitrous gases upon temperature-induced decomposition of metal nitrates probably led to a transport of the molten salt near the surface of the granule. According to the EDX mapping in Fig. 1d, the main part of Pd is also located near the surface. It should be noted that the Pd distribution can only be indicated by the appearance of Pd representing green spots which arise from the low concentration at the detection limit. A line profile of the elemental distribution is given in Fig. S2 showing a depletion of Pd in the core of the granule.

Our TEM investigations demonstrated that the morphology of $CeO_2$ species strongly depends on the catalyst preparation method. Fig. 1e shows a representative TEM image of Pd1/$CeO_2$/PG151. The glass appears as a cloudy grey structure with irregular 15–25 nm $CeO_2$ particles which is in good agreement with the size determined from the XRD investigations (Table 2). Such particles are well attached onto the glass surface. Larger $CeO_2$ particles up to the pore size range are formed after calcination at 900 °C of

tenfold impregnated PG151 (Fig. S3). Compared with the glass-based materials, Pd1/$CeO_2$ appears in TEM as a more irregular material (Fig. S4).

The TEM technique was also applied to estimate the size of Pd species and their distribution. As proven by TEM-EDX elemental mapping (Fig. 1f and Figs. S5–8), Pd is finely distributed and located both on the surface of $CeO_2$ and unloaded glasses. However, in case of Pd1/10$CeO_2$/PG151 the Pd species are exclusively distributed on the metal oxide (Fig. S3). Pd seems to interact well with the defined $CeO_2$ prepared at 900 °C during impregnation, drying and calcination whereas it is not deposited on the glass. A possible reason might be dehydroxylation (removal of silanol groups from the silica surface) [24] which lowers the interactions of the impregnation solution with the silica surface [25,26]. For samples calcined at lower temperature and with lower $CeO_2$ loading, Pd species on the surface of glasses were directly detected by HAADF-STEM. Unfortunately, this technique failed to detect Pd particles of these samples on the surface of $CeO_2$ due to the poor contrast between Pd and Ce. Nevertheless, for Pd1/$CeO_2$/PG151 we estimated the size of Pd particles located on the surface of PG151. Particles of around 2.5 nm were found to populate the glass surface. 7.2% of the particles were below 2 nm and 7.3% where above 3 nm (Figs. S7–9). This result was checked to correlate with CO chemisorption experiments at room temperature where an average diameter of Pd particles is estimated. Noteworthy, this technique has been often applied for such purposes [22].

In order to guarantee metallic state of Pd, all Pd*X*/$CeO_2$/PG*Y* catalysts were initially reduced in a flow of 5 vol% $H_2$ in Ar at 300 °C before the titration tests. It was found, the particle size calculated for Pd1/$CeO_2$/PG151 is in good agreement with that of the visualized Pd species from TEM investigations (Figs. S7–9). Table 2 shows overall surface areas of metallic Pd and average particle sizes determined from CO chemisorption. For the catalysts with an overall Pd loading of approximately 0.6 wt%, this area increases with an increase in surface area of the glasses, while the diameter of Pd particles decreases. As expected, the size of Pd particles in the PG151-based catalysts increases from 2.6 to 5.6 nm with an increase in Pd loading from 0.63 to 5.96 wt%, respectively. Pd dispersion behaves analogously. However, the Pd1/$CeO_2$/PG151 and Pd5/$CeO_2$/PG151 catalysts differ only slightly in the size of Pd particles; 2.6 *vs.* 2.8 nm (Table 2). The classically prepared Pd1/$CeO_2$ possesses Pd particles of 1.6 nm size.

### 3.2. Redox properties of catalytic materials

To derive insights into the reducibility of $PdO_x$/$CeO_2$, we performed $H_2$-TPR measurements. The obtained profiles of hydrogen consumption for all Pd1/$CeO_2$/PGY catalysts as well as for Pd1/$CeO_2$ are shown in Fig. 2. It is obvious that $H_2$ is consumed in three temperature regions. According to several previous studies, they can be assigned to the reduction of: (i) $PdO_x$ below 100 °C [27] and $CeO_2$ in close contact with $PdO_x$ particles between 77 °C and 227 °C [28], (ii) surface $CeO_2$ ($CeO_{2,surf}$) between *ca.* 350 and 550 °C [29,30] and (iii) bulk $CeO_2$ with a maximal $H_2$ consumption at around 800 °C [29,31].

It is worth mentioning that reduction of $PdO_x$ was observed only for Pd1/$CeO_2$ as concluded from the fact that there was a sharp peak of $H_2$ consumption with a maximum of around 100 °C. This is in agreement with previous $H_2$-TPR studies on $PdO_x$/$Al_2O_3$. This process in all other catalysts prepared with the use of glasses probably occurred below 50 °C. The difference between these two types of catalysts may be due to different $PdO_x$-support interactions as the below discussion explains. $PdO_x$ species in all glass-based catalysts are statistically distributed on the surface of $SiO_2$ and also at/on $CeO_2$ species. Contrarily, $PdO_x$ species in Pd1/$CeO_2$ are located directly on the surface of $CeO_2$. According to Muto et al. [32], $PdO_x$ supported on $SiO_2$ (as in case of our glass-based catalysts) are reduced at low temperatures with a maximum of $H_2$ consumption at around 30 °C. Therefore, we were not able to observe this process in all Pd/$CeO_2$/PG materials since 50 °C was the lowest temperature in our $H_2$-TPR tests. Owing to the direct contact of $PdO_x$ with $CeO_2$ in Pd1/$CeO_2$, the reduction of $PdO_x$ species is shifted to higher temperatures because lattice oxygen of $CeO_2$ can oxidize their reduced counterparts. The above discussion is indirectly supported by the fact that the reduction of $CeO_2$ in close contact with $PdO_x$ particles in Pd1/$CeO_2$ differed from that in all Pd/$CeO_2$/PG materials. This process typically occurs via spillover mechanism according to which hydrogen is initially activated on metallic palladium and then transferred to ceria [28,33]. The respective temperature range for this reduction step in our study, *i.e.* between 80 and 270 °C, is comparable to the literature [28]. However, the maxima of $H_2$ consumption in the TPR profiles of all Pd/$CeO_2$/PG materials are shifted to lower temperatures compared with those of Pd1/$CeO_2$. This is due to the fact that the formation of metallic Pd, which is required for hydrogen activation and spillover, in the former materials also occurred at lower temperatures.

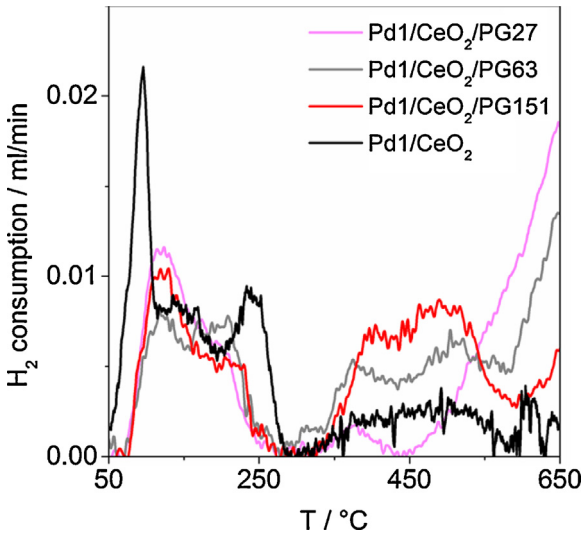


**Fig. 2.** Temperature profiles of hydrogen consumption over Pd1/$CeO_2$/PGY and Pd1/$CeO_2$ catalysts ($H_2$:Ar = 5:95; temperature ramp of 10 °C $min^{-1}$).

The method of catalyst preparation also influences the reducibility of surface $CeO_2$ in the temperature range between 340 and 560 °C. The amount of $H_2$ consumed in this range decreases with a decrease in pore size of the glass support most probably due to an increased $CeO_2$/glass interface leading to lower $CeO_2$ surface areas. For Pd1/$CeO_2$/PG151, only minimal reduction of $CeO_{2,surf}$ takes place in a temperature range of 340 to 440 °C. Pd1/$CeO_2$ also showed a low reducibility of $CeO_{2,surf}$ probably due to the extended coverage of $CeO_2$ with Pd. This statement is supported by the fact that surface reducibility in Pd/$CeO_2$/PG27 materials strongly decreases with an increase in Pd loading (Fig. 3). Bulk $CeO_2$ reduction starts for all catalysts above 560 °C except for Pd1/$CeO_2$/PG27. The bulk $CeO_2$ phase in this catalyst can already be reduced at 450 °C.

### 3.3. Catalytic activity for methane oxidation

To compare catalysts in terms of their activity, methane oxidation tests were performed at a fixed GHSV of ~30.000 $h^{-1}$ in the temperature range between 150 and 550 °C. $CO_2$ was the only gaseous carbon-containing reaction product formed upon $CH_4$ oxidation in excess of oxygen. The unloaded glasses did not show any activity. Thus, the below discussion is related to

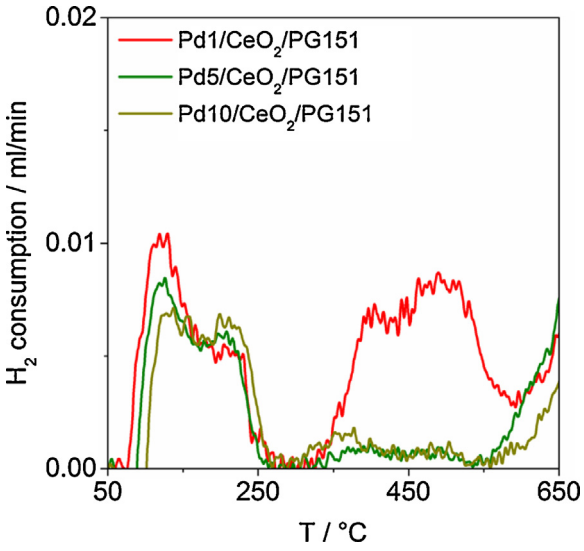


**Fig. 3.** Temperature profiles of hydrogen consumption over PdX/$CeO_2$/PG151 catalysts ($H_2$:Ar = 5:95; temperature ramp of 10 °C $min^{-1}$).

the effect of supporting glasses on the activity of the Pd/$CeO_2$ system. Fig. 4a presents methane conversion in dependence on temperature obtained over differently prepared catalysts possessing around 0.56–1.00 wt% Pd. It is obvious that the glass-free Pd1/$CeO_2$ and $CeO_2$-free Pd1/PG151 catalysts performed similarly to each other but were the least active in the temperature range from 150 to 500 °C. Also si-Pd1/$CeO_2$/PG151 as well

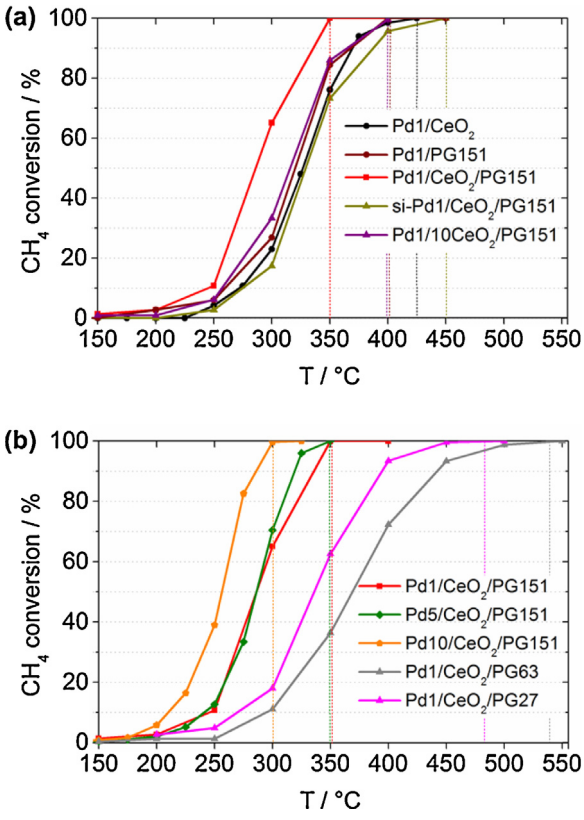


**Fig. 4.** Effect of temperature on methane conversion to $CO_2$ over different PdX/$CeO_2$/PG*Y* catalysts, influence of: (a) different synthesis methods related to reference catalysts Pd1/$CeO_2$ and Pd1/PG151, (b) different size of glass pores and different Pd loading. Reaction conditions: 1.0 vol% $CH_4$ in air, GHSV of ~30.000 $h^{-1}$; repetition experiments have been performed and the differences between measurements were ≤6%.

as Pd1/10$CeO_2$/PG151 do not reveal a remarkable difference but they were slightly more active than Pd1/$CeO_2$ and Pd1/PG151. However, Pd1/$CeO_2$/PG151 containing both Pd and $CeO_2$ on the glass surface was significantly more active and achieved 100% methane conversion at 350 °C. Since Pd1/$CeO_2$ and Pd1/PG151 were significantly less active, we can safely conclude that there is a synergy effect between Pd/$PdO_x$ species and $CeO_2$ located on the surface of the glass support. Nevertheless, such synergy effect appears to depend on the pore size of the supporting glass. Compared to Pd1/$CeO_2$/PG151, Pd1/$CeO_2$/PG63 reached $T_{100}$ (temperature of 100% methane conversion) at 550 °C, *i.e.* at around 200 °C higher temperature. The Pd1/$CeO_2$/PG27 catalyst completely converted methane at 500 °C (Fig. 4b). The classically prepared Pd1/$CeO_2$ was more active than Pd1/$CeO_2$/PG63 and Pd1/$CeO_2$/PG27 in terms of $T_{100}$.

To check the effect of Pd loading on methane conversion, we prepared PG151-based catalysts possessing 3.07 and 5.96 wt% Pd. Unexpectedly, the activity profiles of Pd1/$CeO_2$/PG151 and Pd5/$CeO_2$/PG151 are very similar (Fig. 4b), while Pd10/$CeO_2$/PG151 showed higher activity with $T_{100}$ being 50 °C lower than for the two latter catalysts. The fundamental origins governing the low-temperature activity of the catalysts studied are thoroughly discussed in the following section together with the results of catalysts characterization described in the preceding section.

During the recording of temperature profiles, at each temperature three measurements were performed within 30 min while a decrease in conversion up to $X_{CH4} \leq 2.0\%$ was observed over time. At low temperatures as well as on Pd/$CeO_2$ this behavior was more significant. For industrial or automotive applications, long-term stability is as much of importance as the activity. Under the aspects of high low-temperature activity, we used Pd10/$CeO_2$/PG151 and Pd1/$CeO_2$/PG151 for catalytic runs over 50 h on stream at $T_{20}$, $T_{100}$ as well as 525 °C. Pd1/$CeO_2$ was also tested for comparative purposes. The methane conversions over time on these catalysts are shown in Fig. 5. At $T_{20}$ Pd1/$CeO_2$/PG151 shows the lowest deactivation compared to Pd10/$CeO_2$/PG151 and Pd1/$CeO_2$ (Fig. 5a). Moreover, as the most important aspect for catalytic post-combustion is complete removal of the pollutant, the catalysts were tested at the temperature where they reach full conversion at $T_{100}$, *i.e.* at 305, 350 and 415 °C for Pd10/$CeO_2$/PG151, Pd1/$CeO_2$/PG151 and Pd1/$CeO_2$, respectively. Again, the Pd1/$CeO_2$/PG151 catalyst revealed only a very small decrease in the conversion with in an average deactivation rate of 0.014%/h. Contrarily, Pd1/$CeO_2$ and Pd10/$CeO_2$/PG151 deactivated with correspondently higher rates of 0.07 and 0.056%/h. To check if the deactivation was caused by sintering of $CeO_2$ and/or Pd particles, we analyzed the used catalysts by XRD and CO chemisorption. No significant changes in these structural characteristics as well as Pd amount were detected on Pd1/$CeO_2$/PG151 as well as on Pd1/$CeO_2$ after the long term tests (Table 2). However, some carbon deposits were found on the surface of these materials as proven by elemental analysis. The carbon content in Pd1/$CeO_2$/PG151 and Pd1/$CeO_2$ after 50 h on methane oxidation was $7 \times 10^{-4}$ and $16 \times 10^{-4}$ g(C)/g(catalyst), respectively. On Pd10/$CeO_2$/PG151 the carbon deposition was in between with a value of $12 \times 10^{-4}$ g(C)/g(catalyst). When comparing these data with the average rate of catalyst deactivation, we put forward that the deactivation is related to deposition of carbon species. The deposition obviously not occurs on the Pd surface since CO chemisorption before and after the long term tests show nearly the same results. Instead, it only can occur on the $CeO_2$ surfaces. It appears that high reducibility of surface $CeO_2$ in Pd1/$CeO_2$/PG151 favors oxidation of carbon deposits thus lowering the rate of their accumulation compared to Pd10/$CeO_2$/PG151 and Pd1/$CeO_2$ where the Pd particles are mostly located on $CeO_2$. Noteworthy, at 525 °C both porous glass stabilized catalysts, Pd1/$CeO_2$/PG151 and Pd10/$CeO_2$/PG151, show no deactivation

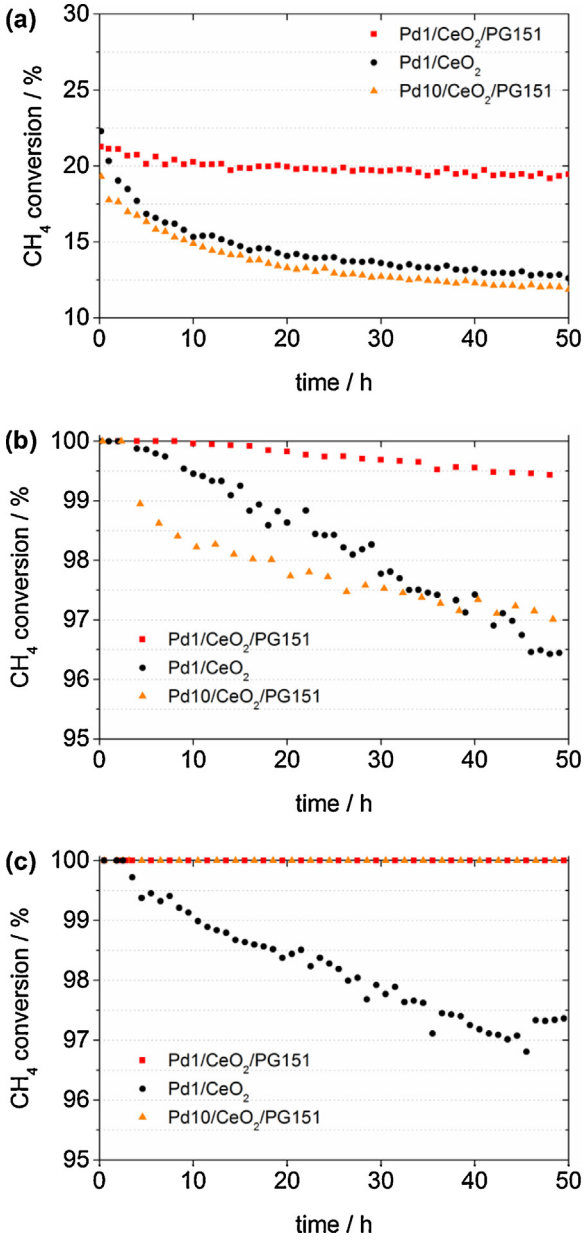


**Fig. 5.** Time on stream methane conversion over $Pd10/CeO_2/PG151$, $Pd1/CeO_2/PG151$ and $Pd1/CeO_2$ at (a) $T_{20}$, (b) $T_{100}$ and (c) 525 °C; reaction conditions: 1.0 vol% $CH_4$ in air, GHSV of ~30.000 $h^{-1}$.

over 50 h on stream while $Pd1/CeO_2$ is deactivated significantly (Fig. 5c).

### 3.4. Origins governing catalyst activity

As demonstrated above, the method of catalyst preparation, Pd content and the kind of porous glasses used as supports strongly influenced catalysts activity for methane combustion. To check the relationship between the size of Pd species and methane oxidation, we compared our catalysts in terms of intrinsic activity of Pd species. For this purpose, we calculated the apparent turnover frequency (TOF) of methane oxidation using conversion data at 250 °C and the number of available surface Pd atoms determined from the amount of irreversibly adsorbed CO. At this temperature, all catalysts showed measurable activity and methane conversion was below 12% with the exception of 40% reached over $Pd10/CeO_2/PG151$. Consequently, the latter TOF can be

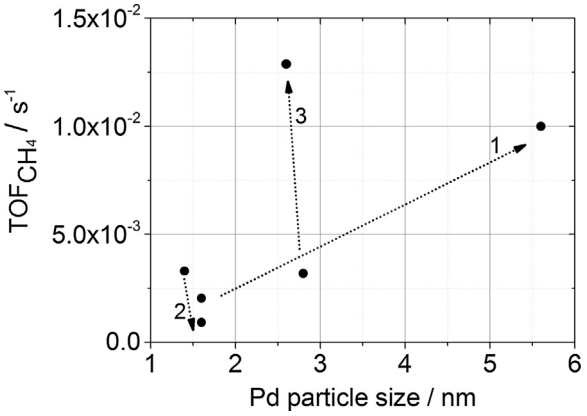


**Fig. 6.** TOF values for methane conversion in dependence on size of Pd particles (arrow 1 = increase in particle size; arrows 2 and 3 = increase in $CeO_{2,surf}$ reducibility).

underestimated because this test was not performed in a differential reactor. Fig. 6 shows the TOF values *vs.* the size of Pd particles. Since no direct relationship could be established we put forward that the size is not the only activity-governing factor.

Taking into account that the mixed Pd/PdO state determines the rate of methane oxidation [34–36], we first turn our attention to mechanistic aspects of Pd oxidation. An oxygen transfer from $CeO_2$ to precious metal keeps the redox Pd/PdO couple alive during the reaction [37]. The contribution of lattice oxygen of the support to this redox process was experimentally proven by means of oxygen isotope exchange experiments [35,38]. Furthermore, Müller et al. evidenced the role of lattice oxygen on the oxidation as well as oxygen exchange of formed carbon dioxide with the catalysts [39,40]. According to theoretical calculations of van Santen [41] large metal nanoparticles are required to activate $\pi$ bonds as in the $O_2$ molecule and a reaction center with unique configuration of several metal atoms is required. This is probably a reason for the increase in TOF over $Pd5/CeO_2/PG151$ and $Pd10/CeO_2/PG151$ possessing larger Pd particles than $Pd1/CeO_2$ (Fig. 6, arrow 1). Incidentally, the larger Pd particles in Pd1/PG151 cause a comparable performance as $Pd1/CeO_2$ even without the redox active metal oxide (Fig. 4a and Fig. S10). In comparison, Fujimoto et al. found a nearly linear increase in the turnover frequency with increasing Pd particle sizes from 3 to 11 nm on $ZrO_2$ [42]. The activity was suggested to directly correlate with oxygen vacancies being present on the $PdO_x$ surface which are preferably formed on larger particles due to their weaker Pd—O bonds. Roth et al. [43] differentiate between 'small' and large Pd particles on alumina. Small particles, below 12 nm, also show a significant increase in activity with increasing particle size while the TOF of particles above 12 nm drops and then stays constant. The increasing activity of 'small particles' with their size is discussed to depend either on decreasing strength of Pd—O bonds with particle size or on the participation of subsurface oxygen atoms on the reaction. Since the catalytic activity of 'large particles' mainly depends on surface PdO on a Pd metal core geometric properties of the Pd/PdO particles determine the activity [43].

For our catalysts with small Pd particles between 1.4 and 1.6 nm, the $CeO_{2,surf}$ reducibility increases in the following sequence: $Pd1/CeO_2/PG27 < Pd1/CeO_2 < Pd1/CeO_2/PG63$ (Fig. 6, arrow 2). As previously reported by Roth et al. [43] small $PdO_x$ particles are more stable against reduction than larger ones and they consequently possess a lower catalytic activity. In our case $PdO_x$ in $Pd1/CeO_2/PG63$ (~1.6 nm) is stabilized against reduction owing to high $CeO_{2,surf}$ redox activity. As a consequence, this catalyst showed lower activity than $Pd1/CeO_2/PG27$ and $Pd1/CeO_2$, which revealed lower $CeO_{2,surf}$ reducibilities. More importantly,

comparing $Pd1/CeO_2$/PG151 and $Pd5/CeO_2$/PG151 catalysts with larger Pd particles of 2.6 and 2.8 nm, respectively, a reversed behavior is shown. $Pd1/CeO_2$/PG151 possesses a *ca.* 4 times higher activity compared to $Pd5/CeO_2$/PG151 (Fig. 6, arrow 3). In this case, catalyst activity increases with higher $CeO_{2,surf}$ reducibility. The larger size of the $PdO_x$ particles in $Pd1/CeO_2$/PG151 (~2.6 nm) enables an improved catalytic redox process due to weaker Pd—O bonds. On the basis of these data we put forward that in case of $Pd1/CeO_2$/PG151 $CeO_2$ efficiently provides oxygen for the reoxidation of Pd to PdO leading to the higher TOF. Furthermore, the oxidation of $CH_x$ fragments formed upon activation of gas-phase $CH_4$ on this catalyst surface is improved leading to enhanced long term stability. The porous glass provides an ideal framework for such complex interactions.

## 4. Conclusion

Porous glasses have been demonstrated to be effective catalyst supports for the $Pd/CeO_2$ system used for complete methane oxidation. The activity of the supported catalysts is governed by the interplay between the size of Pd particles and the $CeO_2$ surface reducibility. These parameters can be tuned by a proper choice of the supporting glass and the method of deposition of Pd and $CeO_2$, which determine the contact between these two active components. The surface area of the porous glass and the Pd loading determine the activity relevant Pd particle size. The surface coverage with Pd particles influences the pure $CeO_{2,surf}$ reducibility. An increase in activity of 2.6 nm $PdO_x$ particles by a factor of 4 could be achieved by the provision of surface oxygen from $CeO_2$ to the catalytic reaction. The porous glass support mediates this interplay. The results could help to reduce noble metal contents for combustion catalysts.

## Acknowledgements

The authors would like to thank Dr. A. Qiao and K. Struve for BET surface area determination, W. Winkler and Dr. M. Schneider for X-ray diffraction analysis, and S. Evert and Dr. H. Atia for CO-chemisorption measurements. We acknowledge the help of J. Ackermann from the application center of Carl Zeiss Microscopy GmbH, Oberkochen, Germany and Dr. M. Frank for his helpful advice.

## Appendix A. Supplementary data

Supplementary data associated with this article can be found, in the online version, at http://dx.doi.org/10.1016/j.apcatb.2015.05.028

## References

[1] P. Forster, V. Ramaswamy, P. Artaxo, T. Berntsen, R. Betts, D.W. Fahey, J. Haywood, J. Lean, D.C. Lowe, G. Myhre, J. Nganga, R. Prinn, G. Raga, M. Schulz, R. Van Dorland, In: S. Solomon, D. Qin, M. Manning, Z. Chen, M. Marquis, K.B. Averyt, M. Tignor, H.L. Miller (Eds.), Climate Change 2007: The Physical Science Basis. Contribution of Working Group I to the Fourth Assessment Report of the Intergovernmental Panel on Climate Change, Cambridge, United Kingdom and New York, USA, 2007, 212.
[2] P. Gélin, M. Primet, Appl. Catal. B: Environ. 39 (2002) 1–37.
[3] G.B. Hoflund, Z.H. Li, J. Nat. Gas Chem. 12 (2003) 153–160.
[4] L.S. Escandón, S. Ordóñez, A. Vega, F.V. Díez, Chemosphere 58 (2005) 9–17.
[5] N. van Vegten, M. Maciejewski, F. Krumeich, A. Baiker, Appl. Catal. B 93 (2009) 38–49.
[6] K. Eguchi, H. Arai, Appl. Catal. A 222 (2001) 359–367.
[7] R.J. Farrauto, J.K. Lampert, M.C. Hobson, E.M. Waterman, Appl. Catal. B: Environ. 6 (1995) 263–270.
[8] L.-H. Xiao, K.-P. Sun, X.-L. Xu, X.-N. Li, Catal Commun. 6 (2005) 796–801.
[9] K. Yasuda, T. Masui, T. Miyamoto, N. Imanaka, J. Mater. Sci. 46 (2011) 4046–4052.
[10] M. Cargnello, J.J.D. Jaén, J.C.H. Garrido, K. Bakhmutsky, T. Montini, J.J.C. Gámez, R.J. Gorte, P. Fornasiero, Science 337 (2012) 713–717.
[11] J. Bassil, A. AlBarazi, P. Da Costa, M. Boutros, Catal. Today 176 (2011) 36–40.
[12] A.M. Venezia, G. Di Carlo, L.F. Liotta, G. Pantaleo, M. Kantcheva, Appl. Catal. B 106 (2011) 529–539.
[13] J.-H. Park, B. Kim, C.-H. Shin, G. Seo, S.H. Kim, S.B. Hong, Top. Catal. 52 (2009) 27–34.
[14] D. Enke, F. Janowski, W. Schwieger, Micropor. Mesopor. Mater. 60 (2003) 19–30.
[15] K.S.W. Schüth, J. Sing, Handbook of Porous Solids, Wiley-VCH, 2002, 2015.
[16] Y.M. Sun, S.J. Khang, Ind. Eng. Chem. Res. 27 (1988) 1136–1142.
[17] J. Li, A.W.-H. Mau, C.R. Strauss, Chem. Commun. (1997) 1275–1276.
[18] I. Chistovskaya, F. Janowski, React. Kinet. Catal. Lett. 43 (1991) 277–282.
[19] S. Wohlrab, A. Janz, M.-M. Pohl, S. Kreft, D. Enke, A. Koeckritz, A. Martin, B. Luecke, Stud. Surf. Sci. Catal. 175 (2010) 315–319.
[20] P. Scherrer, Nachrichten von der Gesellschaft der Wissenschaften zu Göttingen, Mathematisch-Physikalische Klasse (1918) 98–100.
[21] S. Narayanan, K. Krishna, Appl. Catal. A: Gen. 174 (1998) 221–229.
[22] K.N.K. Nakai, Pulse chemisorption measurement <Metal dispersion measurement>, BEL-CAT Application Note: CAT-APP-002 (2003) 1–6.
[23] D.A.M. Monti, A. Baiker, J. Catal. 83 (1983) 323–335.
[24] L.T. Zhuravlev, Colloids Surf. A: Physicochem. Eng. Aspects 173 (2000) 1–38.
[25] C.G. Pope, J. Colloid Interface Sci. 116 (1987) 221–223.
[26] Y. Hirama, T. Takahashi, M. Hino, T. Sato, J. Colloid Interface Sci. 184 (1996) 349–359.
[27] H. Lieske, J. Voelter, J. Phys. Chem. 89 (1985) 1841–1842.
[28] A. Leitenburg, J. Catal. 166 (1997) 98–107.
[29] H.C. Yao, Y.F.Y. Yao, J. Catal. 86 (1984) 254–265.
[30] R. Sasikala, N.M. Gupta, S.K. Kulshreshtha, Catal. Lett. 71 (2001) 69–73.
[31] V. Ferrer, A. Moronta, J. Sanchez, R. Solano, S. Bernal, D. Finol, Catal. Today 107–08 (2005) 487–492.
[32] K.-I. Muto, N. Katada, M. Niwa, Applied Catalysis A: General 134 (1996) 203–215.
[33] A. Bensalem, F. Bozon-Verduraz, V. Perrichon, J. Chem. Soc. Faraday Trans. 91 (1995) 2185–2189.
[34] M. Lyubovsky, L. Pfefferle, Appl. Catal. A: General 173 (1998) 107–119.
[35] D. Ciuparu, F. Bozon-Verduraz, L. Pfefferle, J. Phys. Chem. B 106 (2002) 3434–3442.
[36] A.K. Datye, J. Bravo, T.R. Nelson, P. Atanasova, M. Lyubovsky, L. Pfefferle, Appl. Catal. A: Gen. 198 (2000) 179–196.
[37] R.J. Gorte, AIChE J. 56 (2010) 1126–1135.
[38] W.R. Schwartz, L.D. Pfefferle, J. Phys. Chem. C 116 (2012) 8571–8578.
[39] C.A. Müller, M. Maciejewski, R.A. Koeppel, R. Tschan, A. Baiker, J. Phys. Chem. 100 (1996) 20006–20014.
[40] C.A. Müller, M. Maciejewski, R.A. Koeppel, A. Baiker, Catal. Today 47 (1999) 245–252.
[41] R.A. Van Santen, Acc. Chem. Res. 42 (2008) 57–66.
[42] K.-I. Fujimoto, F.H. Ribeiro, M. Avalos-Borja, E. Iglesia, Journal of Catalysis 179 (1998) 431–442.
[43] D. Roth, P. Gélin, A. Kaddouri, E. Garbowski, M. Primet, E. Tena, Catal. Today 112 (2006) 134–138.